Dielectric response of fully and partially depleted ferroelectric thin films and inversion of the thickness effect

I. B. Misirlioglu, M. Yildiz

Faculty of Engineering and Natural Sciences, Sabancı University, Orhanlı/Tuzla 34956 Istanbul, Turkey

Abstract

We study the effect of full and partial depletion on the dielectric response characteristics of ferroelectric thin films with impurities via a computational approach. Using a thermodynamic approach along with the fundamental equations for semiconductors, we show that films with partial depletion display unique features and an enhanced dielectric response compared to those fully depleted. We find that the capacitance peak at switching can be significantly suppressed in the case of high impurity densities ($>10^{25}/m^3$) with relatively low ionization energy, at the order of 0.5 *eV*. For conserved number of species in films, electromigration of ionized impurities at room temperature is negligible and has nearly no effect on the dielectric response. In films with high impurity density, the dielectric response at zero bias is enhanced with respect to charge-free films or those with relatively low impurity density ($<10^{24}$ $/m^3$). We demonstrate that partially depleted films should be expected to exhibit peculiar capacitance-voltage characteristics at low and high bias and that the thickness effect probed in experiments in ferroelectric thin films could be entirely inverted in thin films with depletion charges where a higher dielectric response can be measured in thicker films. Therefore, depletion charge densities in ferroelectric thin films should be estimated before size-effect related studies. We finally noticed that these findings are in good qualitative agreement with dielectric measurements done on $PbZr_xTi_{1-x}O_3$.

Introduction

Ferroelectric materials in thin film form have been analyzed both phenomenologically and by means of first principles calculations to determine the stability of the polar state against the non-polar state at reduced thickness employing various film-electrode interface states as boundary conditions.[1-13] Among numerous reports whose details are not possible to mention here, the common consensus is that the intrinsic size limit to ferroelectricity is a result of competing phenomena strongly dependent on relaxation of electrostatic energy, metal-film interface electronic character and boundary conditions, strain and electrical domain formation. [2, 3, 6, 14-27] Effects of the Schottky character of the film-electrode interfaces and effects of polarization on band bending have also been considered altough these studies were not emphasizing size effects but rather the effect of electrode types. [27, 28-31] Similar to other types of dielectric thin films, ferroelectrics are highly susceptible to capture of impurities and vacancy formation during fabrication. Below the Curie temperature, in addition to the thickness driven stability, the polar state of a ferroelectric film is highly sensitive to the presence of impurity defects especially due to strong coupling of the polarization to long-range fields these defects create when acting as charge centers. Defects with charges near the surfaces have been corroborated as centers strongly influencing switching characteristics or hinder domain wall motion. [32-36] As with any other wide bandgap semiconductor, these point defects, called impurities in the rest of the work, might act as donors or acceptors in a ferroelectric depending on their valence state and their ionization energies in the crystal with respect to the bottom (top) of the conduction (valence) band.

Injection of charges from the electrodes into the film volume and trapping of these charges at deep or shallow levels by impurities can also determine whether thermally assisted or voltage driven currents (that of Poole-Frenkel type) will prevail during an experimental measurement. It is also well-known that high densities of depletion charges might also reduce the Curie temperature and coercive fields. [37, 38-40]

In spite of a plethora of studies discussing how the ferroelectric state can be tailored, the naturally forming depletion charges due to ionization of impurities creating shallow levels or vacancies accepting/donating carriers in the system have put serious limitations on reliability and functionality. Shallow level impurity effects in ferroelectrics have been computationally studied mostly with emphasis on their impact on the domain structures, domain pinning [32, 41-43] and hystereses. [33, 40, 44-46] Among these works, Xiao et al. [41] previously showed that 180° electrical domain walls are free of oxygen vacancies acting as donors while, in contrast to what has been thought, elastic 90° domain walls can be decorated with these defects and the same conclusion was reached in Ref. 42. In a following study, the interaction of defect dipoles with 90° domain walls leading to the recovery of the electromechanical response was claimed to be the mechanism for the domain memory effect. [43] Double hysteresis loops, obtained for films with high density of defect dipoles in Ref. 43, were experimentally demonstrated in a study the same year. [47] Moreover, loss of switchable polarization and slanting of the hysteresis under cyclic fields due to charge trapping at deep levels that pin the local dipoles is also a direct consequence of presence of impurities and A-site or oxygen vacancies. [48, 49] Semiconductor-ferroelectric and half metal-incipient ferroelectric structures have also been considered wherein it was shown that space charges forming

following band bending upon contact can lead to polarization existence in an incipient ferroelectric such as $SrTiO_3$ in addition to smearing effects considered also in this work as will be demonstrated. [24] Very recently, impact of misfit strain on the spatial free carrier distribution was demonstrated where the charge density can be asymmetrical at top free and bottom grounded surfaces. [50]

Although the real hysteresis behavior [51] is one of the foot prints of ferroelectricity, this characteristic is highly susceptible to detoriation in the presence of depletion charges due to impurities or vacancies. This detoriation originates both from the built-in polarization as well as the passage of leakage currents mostly via the *n*-type or *p*-type carriers introduced into the conduction or valence band respectively, heavily screening or overwhelming or even obscuring the measurement of charge flow in experiments due to changes in the dipolar configuration under external bias.

Despite the aforementioned scenarios for ferroelectric films with depletion charge, the global dielectric response from such structures can still display highly non-conventional behavior as it can naturally be thought that the capacitance measured in an experiment will contain the dipolar and the possible depletion layer shift related response. Capacitance-voltage experiments in films with depletion charges is a well-practiced way of detecting the presence of ferroelectricity as the instability at the coercive field in a ferroelectric crystal produces very large displacement currents which can be higher than the leakage currents and signal the presence of ferroelectric dipoles via the characteristic butterfly shape loops. One measures the "global" dielectric displacement of the structure both to probe hysteresis loops or capacitance in an experiment via the current flowing in and out of the specimen. Therefore, one can talk about only an "effective dielectric

response" of the entire capacitor, which we denote as ε_{eff}, and still not know whether it solely originates from the ferroelectric dipoles. A striking example to such behavior is the very large dielectric response from ferroelectric films with partial electrode screening leading to 180° domains where the dielectric response of the system is determined by the domain wall motion while the real dielectric constant inside each domain is almost the same as the single domain with ideal electrodes. [52] A film structure with a depletion zone near one or both electrode interfaces will have a dielectric response different from a charge-free film that would come only from the ferroelectric dipoles and it is reasonable to think that, due to the shift of the boundary of the depletion zone with applied bias, a contribution from the change in the volumetric configuration of depletion charges is possible at non-zero bias. However, such an effect mostly impacts the spatial dependence of ferroelectric polarization and the dielectric response majorly depends on this component as we shall show.

In this article, we develop a computational approach to understand the effect of the depletion zone particularly on the dielectric characteristics and its shift along the film thickness under applied bias in ferroelectric films starting with fundamental equations of electrostatics within the metal-semiconductor-metal junction formalism. The energetics of the ferroelectric film is incorporated into the approach via a Landau-Ginzburg potential that also accounts for the presence of impurities or vacancies via the energy of mixing at low concentrations. We emphasize and elaborate on the effective dielectric response-voltage ($\varepsilon_{eff} - V$) curves where the effective dielectric response is enhanced particularly at high impurity density in thicker films with respect to thinner ones, in contrast to what one would expect keeping in mind the size effect. We address certain

differences in the hystereses and $\varepsilon_{eff} - V$ behavior of fully depleted and partially depleted films under applied bias and show that films with high depletion charges, hence partial depletion, have a steeper slope in their $\varepsilon_{eff} - V$ curves compared to a fully depleted film. Films with high depletion charge can exhibit "charge induced domains" and have an antiferroelectric-like hysteresis. Finally, we discuss the impact of the polarization magnitude and the smearing of the transition on the depletion zone characteristics at room temperature by repeating the calculations for films with partially relieved internal misfit stresses. [001] $BaTiO_3$ on [001] $SrTiO_3$ single crystal substrates with Pt electrodes are used to demonstrate our approach, focusing our attention on differential capacitance of films with depletion charges.

Theory and Methodology

A wide bandgap ferroelectric with an impurity or concentration density N_D will contain both free carriers and ions originating from ionization of these impurities in the lattice. We consider impurities that donate electrons to the conduction band and they themselves become positive ions. The approach presented is general and can easily be adapted to a *p*-type ferroelectric film through modification of Eqs. 1-4 once the acceptor levels and the Fermi level are specified. The total charge in the system will be dominated by the electrons in the conduction band and the positive ions that have donated these electrons into the conduction band as the intrinsic carriers will be negligible due to the wide bandgap of the ferroelectric. Note that the number of negative charges and positive

charges will be equal in the entire system but not necessarily at the local level. The spatial volumetric density of ionized donor impurities, N_D^+, will be

$$N_D^+ = \frac{N_D}{1 + g_D \exp[q(E_F - E_D - \phi)/kT]} \tag{1}$$

where g_D is ground state degeneracy of the semiconductor (2 in our case), q is the electron charge, E_F is the position of the Fermi energy level within the bandgap that lies between the donor states and similarly E_D is the donor level, ϕ is the local electrostatic potential, k is the Boltzmann constant, T is temperature in Kelvin. The density of electrons in the conduction band, n^-, is equal to the population density in the conduction band given by

$$n^- = N_C \exp\left[\frac{q(E_C - E_F - \phi)}{kT}\right] \tag{2}$$

with N_C being the effective density of states of the conduction band, E_C is the energy level of the bottom of the conduction band (vacuum level taken as zero), Note that if N_D is zero, then the population density of carriers in the conduction band will be equal to the intrinsic carrier density where $n^- = p^+$ with p^+ being the hole density in the valence band. For the system at hand, the Gauss's law for electricity

$$\nabla \cdot \vec{\mathbf{D}} = \rho \tag{3}$$

has to be satisfied where $\vec{\mathbf{D}} = D_x\vec{\mathbf{e}}_x + D_z\vec{\mathbf{e}}_z$, $D_x = \varepsilon_o\varepsilon_b E_x + P_x$ and $D_z = \varepsilon_o\varepsilon_b E_z + P_z$. Here $\vec{\mathbf{D}}$ is the dielectric displacement vector, ε_o is the permittivity of vacuum and ε_b is the background dielectric constant (7 in this work [53]), E_x and E_z are respectively the $x-$ and $y-$ components of the the electric field vector $\vec{\mathbf{E}}$, which can be determined

from $E_x = -\partial\phi / \partial x$ and $E_z = -\partial\phi / \partial z$, P_x and P_z are the components of ferroelectric polarization vector along *x* and *z* directions, respectively. ρ is the total charge density in the system expressed as

$$\rho = N_D^+ + n^- + p^+ \tag{4}$$

for a semiconductor with donor impurities and no acceptor impurities or defects present. The last term of the r.h.s. of (4) is negligible for the test case studied here as the bandgap of the ferroelectric is quite large to produce holes comparable in density to donated carriers and that these holes will be filled by electrons in the conduction band. The transport of impurities is described by the conservation of species equation combined with the so-called constitive relation known as the Nernst–Planck equation, which is used to describe the motion of species under the influence of both the concentration gradient and electric field. The conservation equation for species can be written as

$$\frac{\partial N_D}{\partial t} + \nabla \cdot \vec{\mathbf{J}} = 0 \tag{5}$$

where $\vec{\mathbf{J}}$ is the impurity flux both due to the concentration gradient and electric field driven diffusion of impurities, which can be defined as

$$\vec{\mathbf{J}} = -D\nabla N_D - \beta z N_D \nabla \left(f\phi \right) \tag{6}$$

that extends Fick's first law of diffusion to the case where the diffusing species are also transported due to the gradient in the electrical potential (electromigration). Here, *D* is diffusivity, β is the ionic mobility related to the diffusivity through the Einstein relation as $D = \beta k_B T / q$, and f is the probability of ionization of the impurity given by

$$f = \{1 + g_D \exp[q(E_F - E_D - \phi) / kT]\}^{-1} \tag{7}$$

Eq. 5 is solved with with periodic boundary conditions on the vertical boundaries, and zero flux boundary condition, $\vec{\mathbf{J}}\cdot\vec{\mathbf{n}}$, for the top and bottom boundaries, which can be written as $\frac{1}{N_D}\frac{\partial N_D}{\partial n}=-\frac{\beta z}{D}\frac{\partial\left(f\phi\right)}{\partial n}$ where $\partial/\partial n$ indicates that partial derivatives are evaluated in the unit normal direction. Values used in the formulae up to this point are given in Table 1. The ferroelectric polarization in the dielectric displacement in (3) satisfies the equations of state:

$$\begin{aligned}&2\alpha_3^m P_z+4\alpha_{13}^m P_z P_x^2+4\alpha_{33}^m P_z^3+6\alpha_{111}P_z^5\\&+\alpha_{112}(4P_zP_x^4+8P_z^3P_x^2)+2\alpha_{123}P_zP_x^4-G\left(\frac{\partial^2 P_z}{\partial z^2}+\frac{\partial^2 P_z}{\partial x^2}\right)=-\frac{\partial\phi}{\partial z}\end{aligned} \quad (8a)$$

$$\begin{aligned}&2\alpha_1^m P_x+2(2\alpha_{11}^m+\alpha_{12}^m)P_x^3+2\alpha_{13}^m P_x P_z^2+6\alpha_{111}P_x^5+\\&2\alpha_{112}[3P_x^5+3P_x^3P_z^2+P_xP_z^4]+2\alpha_{123}P_x^3P_z^2-G\left(\frac{\partial^2 P_x}{\partial z^2}+\frac{\partial^2 P_x}{\partial x^2}\right)=-\frac{\partial\phi}{\partial x}\end{aligned} \quad (8b)$$

where α_3^m, α_{13}^m, α_{33}^m, α_1^m, α_{11}^m, α_{12}^m are the renormalized dielectric stiffness coefficients, modified by the misfit strain (-2.56 % for pseudocubic coherent BT on ST) and the two-dimensional clamping of the film, while α_{111}, α_{112}, α_{123} are the dielectric stiffness coefficients in the bulk [55], G is the gradient energy coefficient and is assumed to be isotropic for convenience, with a value of $6\text{x}10^{-10}$ m^3/F. [56] We should remind here that ϕ, N_D, N_D^+, ρ, n^-, components of $\vec{D}$ and P are all field variables and are functions of coordinates. No misfit relaxation mechanism such as dislocation formation is considered as these could compete with the impurity effects and hinder the interpretation of their contribution to the properties probed. Especially inhomogeneous strain fields would significantly alter Eq. 3 owing to the polarization gradient terms forming in the divergence operation and make it very difficult to emphasize depletion charge effects

alone. To account for the potential barrier forming at the film-electrode interfaces upon growth of the ferroelectric on the electroded substrate, we specify the value of this barrier as a variable boundary condition at the electrodes which is modified (lowered or raised) by the application of an external bias, ϕ_{App}, when solving the electrostatic potential of the system. Therefore

$$\phi(z = -L/2, x) = \phi_D - \phi_{App} \text{ and } \phi(z = L/2, x) = \phi_D + \phi_{App} \qquad (9)$$

are the boundary conditions for the electrostatic potential at the film-electrode interfaces employed in our solutions. This means that, in the absence of an external bias, the barrier at the interfaces are updated until convergence while solving the Maxwell equation. As such, a unidirectional polarization in the film that is paralel to the surface normal lowers the barrier on one side while raising it on the other side. The boundary conditions for P_x and P_z are

$$\lambda \frac{\partial P_x}{\partial x} - P_x = 0\Big|_{z=\pm L/2} \text{ and } \lambda \frac{\partial P_z}{\partial z} - P_z = 0\Big|_{z=\pm L/2} \qquad (10)$$

at the top and bottom film-electrode interfaces with λ being the extrapolation length (2 nm in this work for all calculations) and periodic boundary conditions are adopted along the plane of the film. Eq. 10 implies that the ferroelectric polarization at the top and bottom interfaces are suppressed with respect to the interior of the film but this will produce nearly no size effect when moderate-to-high depletion charges are present as we shall demostrate later.

The equations given by 1-8 are solved using a numerical method subject to the BCs in (9) and (10) in a 2D grid $tn \times 160n$ where n is the unitcell length of the grid (0.4 nm in our work) and t is the number of unitcells comprising the film along the thickness.

The initial condition for N_D is a homogeneous distribution and Eq. 5 is solved time dependent and the rest of the variables as time-independent because the time scale for diffusive contribution is much longer than time dependence of the rest of the coordinate variables mentioned above. Hystereses are obtained by plotting the dielectric displacement response of the films to a triangular signal in voltage. To get the $\varepsilon_{eff} - V$ curves, a bias starting from a negative max. voltage drop going towards the positive max. voltage drop at incremental steps of ϕ_{App} is applied to the electrodes which is then reversed to go to zero bias and then end at the max. negative voltage drop where the simulation initially started. We call the initial stage "sweep up" and the following stage "sweep down". At each voltage drop, ϕ_{App}, the average values of $\vec{D}$ and P are recorded by solving Eqs. given by 1-8 whose results are stored for plotting. In obtaining the $\varepsilon_{eff} - V$ data under the signal prescribed above, the solution of the necessary variables at ϕ_{App} is followed by finding values of these variables in the system at $\phi_{App} + \delta\phi$ where $\delta\phi$ is a small signal that (about 1/5000 of the max bias) is chosen to keep the "small signal" electric field value constant for all thicknesses. Then the effective small signal dielectric response along z-axis (film normal) is found from

$$\varepsilon_{eff} = \frac{t\delta\vec{D}}{\varepsilon_0 \delta\phi} \tag{11}$$

where t is film thickness and $\delta\vec{D} = \vec{D}_z\Big|_{(\phi+\delta\phi)} - \vec{D}_z\Big|_{\phi}$ and $\vec{D}_z$ is replaced with P_z when stated for demonstrative purposes. The values of $\vec{D}$ and P_z given above are the averages over the film structures that are used to compute ε_{eff}. Note that Eq. 11 probes the linear response of the systems studied here. All calculations are carried out for room

temperature (RT). To be compatible with experimental notation used in literature, we will replace ϕ_{App} with V in the rest of the paper.

Results and Discussion

Here we discuss the results obtained using the method prescribed in the previous section. RT hystereses and $\varepsilon_{eff} - V$ curves calculated are given in Figures 1a and b for a number of donor impurity densities in a 32 nm thick film. In the case of relatively low donor densities ($\leq 10^{24}$ - 10^{25} /m^3), there is not a distinct difference both in the hystereses and the $\varepsilon_{eff} - V$ curves (See the strong overlap in Figure 2) and ε_{eff} at zero bias is nearly insensitive to depletion charge. The coercive bias in the hystereses is gradually lowering with increasing impurity density as expected. We will discuss the case of the antiferroelectric-like loops shown in Figure 1 in the coming paragraphs as this appears only at rather high impurity densities. At impurity densities of 10^{24}/m^3 and 10^{25}/m^3 the 32 nm film is fully depleted at zero bias and not much of a change is observed in ε_{eff} as seen in Figure 1b. One would anticipate an increase in the dielectric constant at RT for films with the above mentioned impurity densities but the reduction in the Curie point, accompanied by smearing effects, for both impurity densities is not much different than films with no charge. From here onwards we will use the terms “fully” depleted and “partially” depleted for the distribution or formation of ionized impurities at zero bias for a given film thickness. A partially depleted film within the scope of the definition above will have two depletion zones near each electrode. The fully depleted films become partially depleted near one of the interfaces, depending on the bias sign, only at high bias

values but this does not introduce any visible characteristic changes in the $\varepsilon_{eff} - V$ graphs (and therefore what one would expect in *C-V* curves), unlike partially depleted films as discussed in the following paragraphs.

The above picture for the aforementioned impurity densities in 32 nm films can change if impurity density is higher than 10^{25} /m^3, such as 5×10^{25} /m^3 considered here, a close value for instance previously reported for $PbZr_xT_{1-x}O_3$ (PZT) films. [57] A decrease in the coercive bias values is apparent from the hystereses in Figure 1. This is also reflected in the $\varepsilon_{eff} - V$ behavior where the loops shrink but with a concurrent increase in ε_{eff} at zero bias (Figure 1b). Furthermore, that the depletion zones form near both electrode interfaces with a low-charge-density middle section is expected to directly impact the spatial variation of the ferroelectric polarization, leading to a more prominent smearing in the Curie temperature. We must also add here that, during the application of a bias in particular, the impurities do not undergo a distingusihable redistribution in the film volume resulting from the diffusion equation in Eq. 6 because the impurity as well as the ionic mobilities under applied field at RT are very low. The possible variations in electric field due to electromigration has thus nearly zero contribution to the dielectric displacement that establishes the relation between ρ and polarization components. Figure 1a and b show that, for an impurity density as high as 7.5×10^{25}, the coercive bias is much lower compared to films with impurity densities around 10^{24} – 10^{25} with a steeper slope of the $\varepsilon_{eff} - V$ curves near switching. Apart from the formation of depletion zones near top and bottom electrodes, whose widths change with applied bias, we must point out here that the depletion charges or direct depletion zone shifts do not have an influence on the dielectric response exceeding that of coming from the ferroelectric

dipoles: The main contribution to the dielectric response is from the ferroelectric dipoles in all cases whose magnitude couple to the electric field where ascending impurity densities increase the charge density that creates inhomogeneous electric fields inducing rather sharp gradients of polarization and smear T_C. We hereby conclude that the shift of depletion zone impacts $\varepsilon_{eff} - V$ behavior through a spatially varying P_z. Besides, we also note that the contribution from the first term of dielectric displacement (Eq. 3), $t\varepsilon_b\varepsilon_0 dE/\delta\phi$, containing the electric field is nearly constant for all impurity densities being around 10% of the overall response. Keeping in mind that we consider ideal metal electrodes, this result signals in a way the low sensitivity of the dielectric displacement to semiconducting parameters of the ferroelectric such as the impurity density (if not too high) and amount of band bending taking place and that the main contribution comes from ferroelectric polarization. A different conclusion was reached, for instance, by Watanabe [27] in his rigorous treatment of a ferroelectric/insulator/semiconductor structure but one should keep in mind that the electrostatic boundary conditions (that the ferroelectric is either in contact with an insulating thin layer or a doped semiconductor whose bands will align in response to the ferroelectric polarization) in Ref. 27 is entirely different than what is considered in the current work. We give the $\varepsilon_{eff} - V$ plots in Figure 2 for two impurity densities to demonstrate that ferroelectric polarization determines the dielectric response in all cases as well as pointing out some details. Looking at Figure 2a, one important difference between $\delta P_z/\delta\phi$ and $\delta\bar{D}_z/\delta\phi$ displayed is that the $\delta\bar{D}_z/\delta\phi$ exhibits a dip at a particular value of $|\phi_{App}|$ while $\delta P_z/\delta\phi$ has only a slope change at the same bias while no such detail is visible in 2b. Figure 3 displays the

depleted volumes (in the form of a charge density map, namely ρ) at denoted positive bias values from Figure 2a. Examining the distribution of ρ near ±1.6 V where the dip appears in the $\varepsilon_{eff} - V$ curve, we find that it coincides with the disappearance of one of the depletion zones near one of electrode interfaces. In the case of leakage currents, note that such an effect could make a sudden change in the current density measured in experiments as the interface with no depletion zone might behave as Ohmic. Note that the asymmetry in the depletion widths near top and bottom electrodes are due to the sign of the polarization that is positive (pointing upward) as expected and experimentally observed in the early work of Blom et al.. [28]

For impurity densities approaching 2×10^{26} in 32 nm films, the characteristic butterfly shapes of the $\varepsilon_{eff} - V$ are lost. This is because saw tooth type domains are stabilized at low-to-moderate values of bias as mentioned in a very recent work. [40] Moreover, the film at such impurity densities becomes partially depleted. The $\vec{D}_z - V$ behavior of such a thin film with such high density of depletion charge also exhibits an antiferroelectric-like behavior as given in Figure 1. Stabilization of saw tooth-type domains result only in a domain wall motion with low-to-moderate values of applied bias, accompanied by the motion of the border between the depleted volume and the rest of the film, thereby yielding the linear region in the $\vec{D}_z - V$ curve in Figure 1a. Thus, a large apparent dielectric response can be anticipated around zero bias, corresponding to a linear slope of around 250 using $(t/\varepsilon_0)\delta\vec{D}_z/\delta\phi$. This response is much larger than that of the films with lower depletion charge because the former comes from domain wall motion while the latter is a single domain response originating from ratio of the induced dipole

moment to the small bias signal. Note that this behavior cannot directly be compared to that of a multi domain charge-free ferroelectric with dead layers as a charge-free structure will not exhibit switching peaks due to gradual domain wall motion in nearly the entire bias range. Moreover, the spatial distribution of the internal electric fields in a ferroelectric film with depletion charges is very different than a charge-free film with dead layers at the film-electrode interfaces.

To probe the possible impact of film thickness on the coupling between depletion charges and capacitance under applied bias from which we extract ε_{eff}, we repeat the calculations for a 16 nm film for the same impurity densities as before and the $\varepsilon_{eff} - V$ curves for this structure are given in Figure 4. A similar trend to that of the 32 nm films occurs in the curves: The zero bias dielectric response attains higher values with increasing impurity density and the slopes of the curves following switching are strikingly different for films with high densities of impurities. We find out, however, that the ε_{eff} values overall for the 16 nm and 32 nm films are significantly different especially for a high impurity density and this is because the thicker films become partially depleted with depletion zones at the electrode interfaces while the the 16 nm remains fully depleted nearly in the entire bias for the impurity densities considered. In order to exemplify this, we provide Figure 5 for comparison. For an impurity density of 5×10^{25}, the $\varepsilon_{eff} - V$ curves of the 32 nm and 16 nm films are plotted in Figure 5a. It is clear that the 32 nm film has a higher zero bias dielectric response and it switches at a lower bias (meaning as well a much lower coercive electric field) indicating a lowered, or "softer" overall polarization with respect to the charge free case. Such a thickness effect is in full contrast with films having low or no depletion charge and is discussed in more detail in

the coming paragraphs. Increasing the impurity density to 7.5×10^{25} /m^3 (Figure 5b) puts the 16 nm film in the partial depletion regime but the 32 nm film has still a higher ε_{eff} in addition to a significantly reduced coercive bias, even lower than the 16 nm film, pointing out the strong impact of the depletion charge induced fields that are higher near the electrode interfaces with respect to the 16 nm film. We skip at the moment thinner films, such as the 8 nm one after noticing that the $\varepsilon_{eff}-V$ curves follow completely the same trend, but with different values of course, as that of the 16 nm one, although we do give ε_{eff} for the 8 nm films in comparison with thicker ones with various impurity densities to reveal its dependence on thickness in the presence of impurities, which we discuss in the next paragraph.

ε_{eff} calculated using Eq. 11 at zero bias for the 32 nm thick, 16 nm thick and the 8 nm thick films are provided in Figure 6 as a function of impurity density. We include the 8 nm thick films here that do not exhibit any partial depletion for the entire range of impurity densities probed to reveal the trend with reduced thickness. It is very important to note that, for the same impurity density, the thicker film has a higher effective dielectric response than the thinner one when impurity density is high. This is an interesting finding of our study: If one envisions the possible impact of a size effect, a thinner film would be expected to yield a larger dielectric response compared to a thicker one as the thinner film would be expected to have a lower Curie temperature and a lower polarization under the BCs given in Eq. 10 that are customarily used in calculations. However, the thicker film with high impurity density does have a higher dielectric response because of the large variation of the built-in field with thickness particularly in the partially depleted volume, hence steeper spatial gradients of polarization, leading to a

possible visible smearing of T_C with respect to the thinner film. We do check whether such behavior is due to a "smearing of T_C" in the thicker film with respect to the thinner 16 nm one and confirm that this is exactly the case (See Figure 7). Average of the absolute value of ferroelectric polarization at each coordinate, $<|P|>$, is given in Figure 7 to avoid misinterpretation of the transition characteristics as multidomains become stable in films with high charge densities in addition to the multidomain state stabilizing around 400K in the 8 nm film due to the polarization boundary conditions (This is not an impurity effect as the same behavior is observed in the charge-free film). [58] The smearing is visible in the 32 nm film having a 10^{26} impurities/m^3 and is dramatic for the same thickness having 2×10^{26} impurities/m^3 with considerable reduction of polarization around RT. This reduction is lower in 16 nm films while it is barely visible in the 8 nm film. In the case of high impurity densities the change in polarization of the 8 nm thick film is hardly noticable as seen in the plots. There is also a noticable drop in T_C of the 32 nm film for 10^{26} impurities/m^3 or higher (shown with the arrows in Figure 7). The phase transition is also sharper for thinner films with high impurity density with respect to thick films, a conclusion also reached in Ref. 27. For impurity densities at the order of 10^{25} or less, all films have the expected thickness-driven behavior. One important feature that we mentioned above and should not escape attention in the plots given in Figure 7 is that the $<|P|>$ makes a slight kink in the 8 nm film around 400K for nearly all impurity densities including no impurity case which we find to be due to a transition into a electrical multidomain state resulting from the value of the extrpolation length we employ (no electrical domains form for relatively large extrapolation lengths such as 10 nm). Such an outcome is possible and is already being considered by some researchers. [58] Moreover,

the values of <|P|> above the T_C come from the built-in, non-ferroelectric polarization in all plots of Figure 7. In the light of the plots given in Figure 7, looking at the values of the dielectric response of the films at low charge densities in Figure 6, one immediately notices that the thicker films have lower dielectric response, indicating a minimal change in T_C due to the depletion charges with respect to the charge-free one and effectively a "sharper" transition, allowing a possible discussion on size-effects solely based on the impact of polarization boundary conditions keeping again in mind that ideal screening of electrodes are considered (i. e. no dead layers). Prior to the submission of this paper, we became aware of a systematic work on thickness effects in the dielectric response. An increase in the measured dielectric constant with thickness was reported for pulsed laser deposition grown PZT films nearly free of 90° domains [58] and such an outcome is qualitatively in very good agreement with the mechanism of enhancement for the effective dielectric response proposed in the current work. Note that thicknesses of the PZT films studied in Ref. 58 other than the ~ 10 nm one are well above the critical thickness for misfit dislocation determined by the STO-PZT lattice misfit, meaning the films are nearly fully relaxed, eliminating the misfit strain relaxation as a dominant mechanism giving rise to the observed trend. The sudden jump in the dielectric constant at some critical thickness range reported in Ref. 58 is probably due to the formation of a low density of elastic *a*-domains but the general enhancement of the dielectric response is still visible at lower thicknesses where *a*-domains are absent. We also observe that the 32 nm film has a visible, steep increase in the dielectric response once the film becomes partially depleted (around 2×10^{25} impurities/m^3) at or above which the 16 nm and 8 nm films remain still fully depleted. One can thus conclude that thicker films that are

partially depleted are under a more profound influence of the depletion charges compared to thinner ones owing to the "higher extent of inhomogeneous built-in fields" in the former. It is tempting to think that the depletion charges or the shift of the depleted volume upon applied bias directly impact the dielectric response via the first term of the dielectric displacement but we demonstrate that the dielectric response is mainly determined by the ferroelectric component. For relatively high depletion charge densities caused by high impurity concentrations (such as $>10^{26}$ impurities/m^3), thicker films are under a heavier influence of the smearing of the transition compared to thinner ones for the same depletion charge density. What one would expect in terms of a thickness effect in charge-free films can be entirely inverted when high densities of depletion charges exist. Therefore, experimental results on size and thickness effects are highly vulnerable to misinterpretation unless one carries out measurements to estimate the depletion charge densities in ferroelectric films. One must be, however, careful in not generalizing this trend to all film thicknesses: A relatively thick film, at the order of several hundred nanometers or a micron or even more, with high depletion charge will have partial depletion and the depletion zone will be confined to the near-electrode regions, rendering most of the interior of the film volume nearly charge-free. Such a film might still behave similar to a charge-free film as long as the charge-free volume is much larger than the depleted volume.

Conclusions

The most important result we obtain from our calculations is that depletion charges, when high in density, lead to an enhancement of the dielectric response of the thicker films at small bias with peculiar behavior near the switching peaks despite the fact that partial or full depletion does not change the max. ionized impurity density. Our findings imply that the thickness effect observed in stability of polarization in charge-free films can be inverted for films with moderate-to-high depletion charges where thicker films have a smeared and possibly reduced Curie temperature (with respect to the charge-free films having the same thickness) contrary to what one would expect under the BCs used for polarization. The predicted increase in the dielectric constant for thicker films in this work is also in qualitative agreement with previously published experimental results. While the hystereses exhibit a shrinkage along the field axis with increasing impurity density, the slopes of the $\varepsilon_{eff} - V$, and therefore the *C*-*V* curves, at various bias values could be evaluated to understand whether the specimen films are fully or partially depleted. We show that fully depleted films display a rather constant slope in $\varepsilon_{eff} - V$ plots near or away from the coercive bias while slope of the $\varepsilon_{eff} - V$ curves are prominently steeper than that of fully depleted films especially near coercive bias values. The reason for the latter is the partial depletion and that the depleted volume at each interface changes with applied bias rendering a significant and continuous change in polarization. In partially depleted films, the transition from a state with depletion zones at both interfaces to a state with only one depletion zone at one of the interfaces displays a characteristic kink at the relevant bias. In the case of very high impurity densities (such as > 10^{26} / m^3), electrical domains are stabilized at low-to-moderate bias leading to an antiferroelectric-like response of the system in the hysteresis plots. The linear $\bar{D}_z - V$

region in the hystereses have a very large apparent dielectric response compared to films in single domain state because this response comes predominantly from domain wall motion.

Acknowledgements

I. B. M. acknowledges the support of the Turkish Academy of Sciences (TÜBA) through GEBİP.

References

[1] Kretschmer R and Binder K, Surface effects on phase transitions in ferroelectric and dipolar magnets1979 *Phys. Rev. B* **20** 1065.

[2] Bratkovsky A M and Levanyuk A P, 2000 Abrupt appearance of the domain pattern and fatigue of thin ferroelectric films *Phys. Rev. Lett.* **84**, 3177-80

[3] Junquera J and Ghosez P 2003 Critical thickness for ferroelectricity in perovskite ultrathin films *Nature* **422** 506-9

[4] Ahn C H, Rabe K M and Triscone J M, 2004 Ferroelectricity at the nanoscale: Local polarization in oxide thin films and heterostructures *Science* **303** 488-91

[5] Kim D J, Jo J Y, Kim Y S, Chang Y J, Lee J S, Yoon J G, Song T K and Noh T W 2005 Polarization relaxation induced by a depolarization field in ultrathin ferroelectric BaTiO3 capacitors *Phys. Rev. Lett.* **95** 237602

[6] Sai N, Kolpak A M and Rappe A M 2005 Ferroelectricity in ultrathin perovskite films *Phys. Rev. B* **72** 020101

[7] Tenne D A, Bruchhausen A, Lanzillotti-Kimura N D, Fainstein A, Katiyar R S, Cantarero A, Soukiassian A, Vaithyanathan V, Haeni J H, Tian W, Schlom D G, Choi K J, Kim D M, Eom C B, Sun H P, Pan X Q, Li Y L, Chen L Q, Jia Q X, Nakhmanson S M, Rabe K M and Xi X X, 2006 Probing nanoscale ferroelectricity by ultraviolet Raman spectroscopy *Science* **313** 1614-16

[8] Gerra G, Tagantsev A K, Setter N and Parlinski K 2006 Ionic polarizability of conductive metal oxides and critical thickness for ferroelectricity in BaTiO3 *Phys. Rev. Lett.* **96**, 107603

[9] Yacoby Y, Girshberg Y, Stern E A and Clarke R 2006 Domain structure in ultrathin ferroelectric films: Analysis with a free energy model *Phys. Rev. B* **74** 104113

[10] Nagarajan V, Junquera J, He J Q, Jia C L, Waser R, Lee K, Kim Y K, Baik S, Zhao T, Ramesh R, Ghosez P and Rabe K M 2006 Scaling of structure and electrical properties in ultrathin epitaxial ferroelectric heterostructures *J. Appl. Phys.* **100** 051609

[11] Palova L, Chandra P and Rabe K M 2007 Modeling the dependence of properties of ferroelectric thin film on thickness *Phys. Rev. B* **76** 014112

[12] Paul J, Nishimatsu T, Kawazoe Y and Waghmare U V 2007 Ferroelectric phase transitions in ultrathin films of BaTiO3 *Phys. Rev. Lett.* **99** 077601

[13] Akdogan E K and Safari A 2007 Thermodynamic theory of intrinsic finite-size effects in PbTiO3 nanocrystals. I. Nanoparticle size-dependent tetragonal phase stability *J. Appl. Phys.* **101** 064114

[14] Tagantsev A K, Gerra G and Seter N 2008 Short-range and long-range contributions to the size effect in metal-ferroelectric-metal heterostructures *Phys. Rev. B* **77** 174111

[15] Almahmoud E, Navtsenya Y, Kornev I, Fu H X and Bellaiche L 2004 *Phys. Rev. B* **70** 220102

[16] Dieguez O, Tinte S, Antons A, Bungaro C, Neaton J B, Rabe K M and Vanderbilt D 2004 Ab initio study of the phase diagram of epitaxial BaTiO3 *Phys. Rev. B* **69** 212101

[17] Balzar D, Ramakrishnan P A and Hermann A M 2004 Defect-related lattice strain and the transition temperature in ferroelectric thin films *Phys. Rev. B* **70** 092103

[18] Almahmoud E, Navtsenya Y, Kornev I, Fu H X and Bellaiche L 2004 Properties of Pb(Zr,Ti)O-3 ultrathin films under stress-free and open-circuit electrical boundary conditions *Phys. Rev. B* **70** 220102

[19] Stengel M and Spaldin N A 2006 Origin of the dielectric dead layer in nanoscale capacitors *Nature* **443** 679-82

[20] Yu J, Wu Z, Liu Z, Yan Q, Wu J, Duan W 2008 Phase diagram of ferroelectric BaTiO(3) ultrathin films under open-circuit conditions *J. Phys: Cond. Mat.* **20** 135203

[21] Stengel M, Vanderbilt D and Spaldin N A 2009 Enhancement of ferroelectricity at metal-oxide interfaces *Nature Mat.* **8** 392-7

[22] Okatan M B and Alpay S P 2009 Imprint in ferroelectric materials due to space charges: A theoretical analysis *Appl. Phys. Lett.* **95** 092902

[23] Al-Saidi W, Rappe A M 2010 Density functional study of PbTiO3 nanocapacitors with Pt and Au electrodes *Phys. Rev. B* **82** 155304

[24] Morozovska A N, Eliseev E A, Svechnikov S V, Krutov A D, Shur V Y, Borisevich A Y, Maksymovych P, Kalinin S V 2010 Finite size and intrinsic field effect on the polar-active properties of ferroelectric-semiconductor heterostructures *Phys. Rev. B*. **81**, 205308

[25] Cai M Q, Zheng Y, Ma P- W and Woo C H 2011 Vanishing critical thickness in asymmetric ferroelectric tunnel junctions: First principle simulations *J. Appl. Phys.* **109** 024103

[26] Maksymovych P, Huijben M, Pan M, Jesse S, Balke N, Chu Y.-H, Chang H J, Borisevich A Y, Baddorf A P, Rijnders G, Blank D H A, Ramesh R, and Kalinin S V. 2012 Ultrathin limit and dead-layer effects in local polarization switching of BiFeO3 *Phys. Rev. B* **85** 014119

[27] Watanabe Y 1998 Theoretical stability of the polarization in a thin semiconducting ferroelectric *Phys. Rev. B* **57** 789-804

[28] Blom P. W. M., Wolf R. M., Cillessen J. F. M. and Krijn M. P. C. M. 1994 Ferroelectric schottky diode *Phys. Rev. Lett.* **73** 2107-2110

[29] Matsuura H 2000 Calculation of band bending in ferroelectric semiconductor *New. J. Phys.* **2** 8.1-8.11

[30] Pintilie L and Alexe M 2005 Ferroelectric-metal heterostructures with Schottky contacts. I. Influence of the ferroelectric properties *J. Appl. Phys.* **98** 123103

[31] Pintilie L, Boerasu I, Gomes M J M, Zhao T, Ramesh R, and Alexe M 2005 Metal-ferroelectric-metal structures with Schottky contacts. II. Analysis of the

experimental current-voltage and capacitance-voltage characteristics of Pb(Zr,Ti)O-3 thin films *J. Appl. Phys.* **98** 123104

[32] He L X and Vanderbilt D 2003 First-principles study of oxygen-vacancy pinning of domain walls in PbTiO3 *Phys. Rev. B* **68** 134103

[33] Morozovska A N and Eliseev E A 2004 Modelling of dielectric hysteresis loops in ferroelectric semiconductors with charged defects *J. Phys: Cond. Mat.* **16** 8937-56

[34] Ren X 2004 Large electric-field-induced strain in ferroelectric crystals by point-defect-mediated reversible domain switching *Nat. Mater.* **3** 91-94

[35] Kalinin S V, Jesse S, Rodriguez B J, Chu Y H, Ramesh R, Eliseev E A and Morozovska A N 2008 Probing the role of single defects on the thermodynamics of electric-field induced phase transitions *Phys. Rev. Lett.* **100** 155703

[36] Morozovska A N, Svechnikov S V, Eliseev E A, Rodriguez B J, Jesse S and Kalinin S V 2008 Local polarization switching in the presence of surface-charged defects: Microscopic mechanisms and piezoresponse force spectroscopy observations *Phys. Rev. B* **78** 054101

[37] Bratkovsky A M and Levanyuk A P 2000 Ferroelectric phase transitions in films with depletion charge *Phys. Rev. B.* **61** 15042-50

[38] Zubko P, Jung D J and Scott J F 2006 Space charge effects in ferroelectric thin films *J. Appl. Phys.* **100** 114112

[39] Misirlioglu I B, Okatan M B and Alpay S P 2010 Asymmetric hysteresis loops and smearing of the dielectric anomaly at the transition temperature due to space charges in ferroelectric thin films *J. Appl. Phys.* **108** 034105

[40] Misirlioglu I B, Cologlu H N and Yildiz M 2012 Thickness driven stabilization of saw-tooth-like domains upon phase transitions in ferroelectric thin films with depletion charges *J. Appl. Phys.* **111** 064105

[41] Xiao Y, Shenoy V B and Bhattacharya K 2005 Depletion layers and domain walls in semiconducting ferroelectric thin films *Phys. Rev. Lett.* **95** 247603

[42] Hong L, Soh A K, Du Q G and Li J Y 2008 Interaction of O vacancies and domain structures in single crystal BaTiO(3): Two-dimensional ferroelectric model *Phys. Rev. B* **77** 094104

[43] Zhang Y, Li J and Fang D 2010 Oxygen-vacancy-induced memory effect and large recoverable strain in a barium titanate single crystal *Phys. Rev. B* **82** 064103

[44] Li K T and Lo V C 2005 Simulation of oyxgen vacancy induced phenomena in ferroelectric thin films *J. Appl. Phys.* **97** 034017

[45] Misirlioglu I B and Yildiz M 2012 Polarization retention and switching in ferroelectric nanocapacitors with defects on tensile substrates *Sol. Stat. Elec.* **67** 38

[46] P Suryanarayana, K Bhattacharya 2012 Evolution of polarization and space charges in semiconducting ferroelectrics *J. Appl. Phys.* **111** 034109

[47] Folkman C M, Baek S H, Nelson C T, Jang H W, Tybell T, Pan X Q and Eom C B 2010 Study of defect-dipoles in an epitaxial ferroelectric thin film *Appl. Phys. Lett.* **96** 052903

[48] Tagantsev A K, Stolichnov I, Colla E L and Setter N 2001 Polarization fatigue in ferroelectric films: Basic experimental findings, phenomenological scenarios, and microscopic features *J. Appl. Phys.* **90** 1387-402

[49] Cockayne E and Burton B P 2004 Dipole moment of a Pb-O vacancy pair in PbTiO3 *Phys. Rev.* **69** 144116

[50] Yang L and Dayal K 2012 Influence of strain on space charge distribution at ferroelectric thin-film free surfaces *Acta Mat*. **60** 6457-6463.

[51] Please see "Scott J F 2008 Ferroelectrics go bananas *J. Phys.: Cond. Mat.* **20** 021001" for how non-real hystereses in an ordinary dielectric can emanate.

[52] Bratkovsky A M and Levanyuk A P 2001 Very large dielectric response of thin ferroelectric films with the dead layers *Phys. Rev. B* **63** 132103

[53] Very close values were reported in Hlinka J and Marton P 2006 Phenomenological model of a 90 degrees domain wall in BaTiO3-type ferroelectrics *Phys. Rev. B* **74** 104104 as well as in Tagantsev A K 2008 Landau Expansion for Ferroelectrics: Which Variable to Use? *Ferroelectrics* **375** 19-27

[54] The oxygen mobility given in "Yoo H-I, Chang M-W, Oh T-S, Lee C-E, Becker K D 2007 Electrocoloration and oxygen vacancy mobility of BaTiO3 *J. Appl. Phys.* **102** 093701" was used in this study.

[55] The free energy coefficients are compiled from "Pertsev N A, Zembilgotov A G and Tagantsev A K 1998 Effect of mechanical boundary conditions on phase diagrams of epitaxial ferroelectric thin films *Phys. Rev. Lett.* **80** 1988-91"

[56] Please see the Appendix in "Bratkovsky A M and Levanyuk A P 2009 Continuous Theory of Ferroelectric States in Ultrathin Films with Real Electrodes *J. Comp. Theor. Nano.* **6** 465-89"

[57] Personal communication with Levanyuk A. P., June 2012.

[58] Pintilie L, Vrejoiu I, Hesse D, LeRhun G and Alexe M 2007 Extrinsic contributions to the apparent thickness dependence of the dielectric constant in epitaxial Pb,Zr,TiO_3 thin films *Phys. Rev. B* **75** 224113

Table and Figure Captions

Table 1. Values of the constants and parameters used in solving Eqns. 1-7. Vacuum energy level is zero and all energies are given with respect to vacuum.

Figure 1. (a) Hysteresis loops of the 32 nm film for various impurity densities and (b) their $\varepsilon_{eff} - V$ responses for various impurity densities. The curves for 10^{24} (dashed blue line) and 10^{25} (solid red line) nearly overlap and are difficult to distinguish.

Figure 2. Effective dielectric response obtained using $(t/\varepsilon_0)dD_z/dV$ (solid line) and $(t/\varepsilon_0)dP_z/dV$ (dashed line) on the same plot for (a) impurity density of 5×10^{25} / m^3 and (b) 10^{25} / m^3.

Figure 3. Distribution of ρ at indicated bias voltages in the 32 nm film for an impurity density of 5×10^{25} / m^3. The colorbar scales with 10^6 C/m^3.

Figure 4. $\varepsilon_{eff} - V$ response of the 16 nm films for various impurity densities. Notice the reduction in coercive bias and switching peaks. The curves for 10^{24} (dashed blue line) and 10^{25} (solid red line) nearly overlap and are difficult to distinguish

Figure 5. Comparison of the $\varepsilon_{eff} - V$ responses of the 16 nm (red curve) and 32 nm (black curve) thick films for (a) 5×10^{25} / m^3 and (b) 7.5×10^{25} / m^3 impurity density.

Figure 6. Impurity density dependence of the ε_{eff} response of the 8 nm, 16 nm and 32 nm thick films. The symbols indicate the data points and the lines are guides to the eye.

Figure 7. Temperature dependence of <|P|> for 3 different thickness in case of (a) 5×10^{25} impurities/m^3, (b) 1×10^{26} impurities/m^3, (c) 2×10^{26} impurities/m^3. Note the pronounced reduction in Curie temperature in the 32 nm film with high depletion charge

density with respect to 32 nm charge-free film and those thinner films with the same charge density.

Table 1.

E_F	E_D	E_V ,	E_C	φ (Pt)	β (Ref. 54)
-3.9 eV	-4 eV	-6.6 eV	-3.6 eV	-5.5 eV	$(53/T)\times exp(-1/kT)$

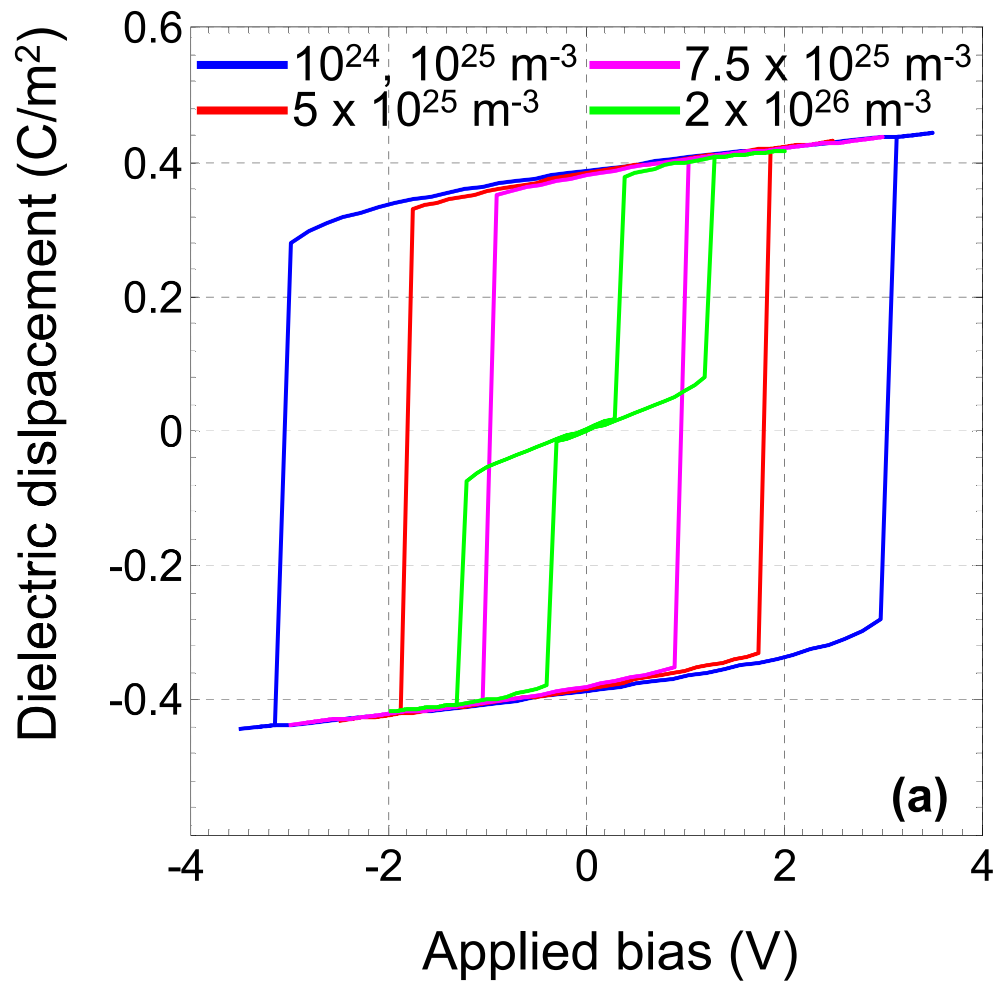

Figure 1a. Misirlioglu and Yildiz

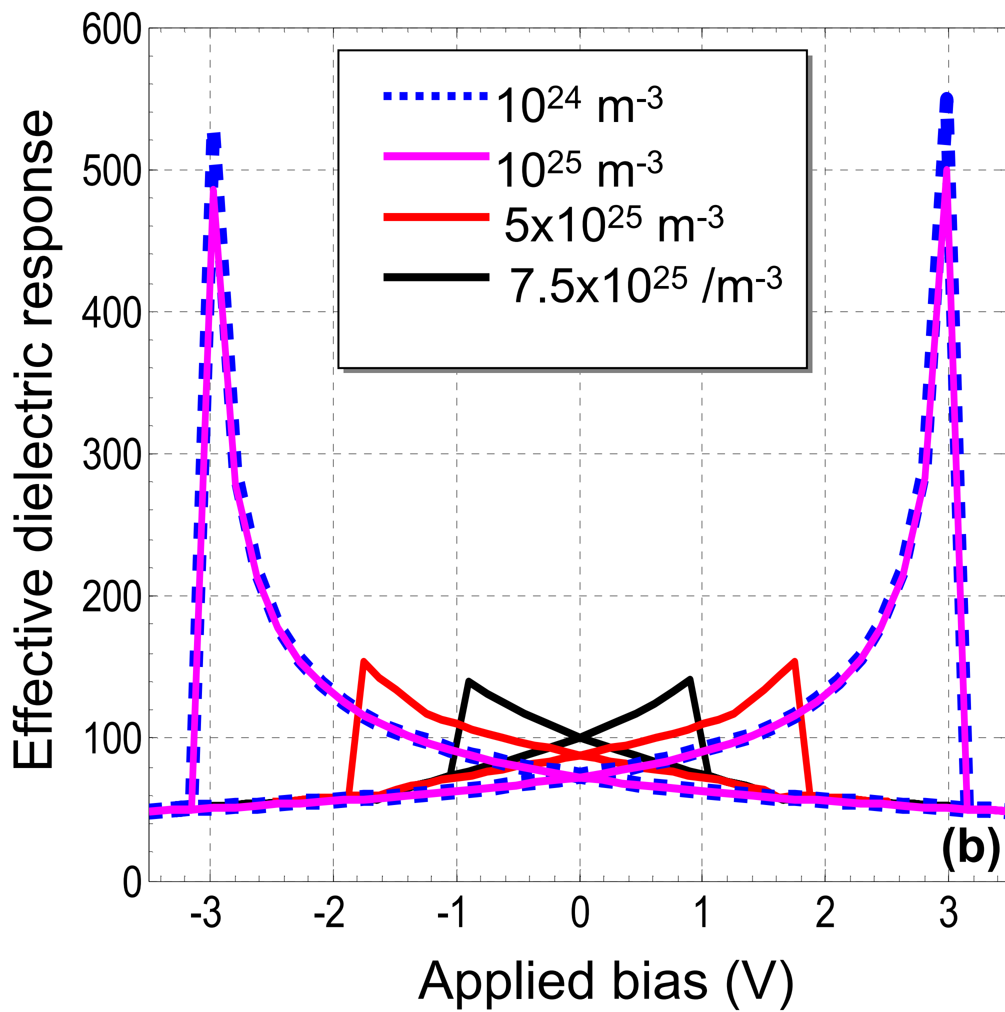

Figure 1b. Misirlioglu and Yildiz

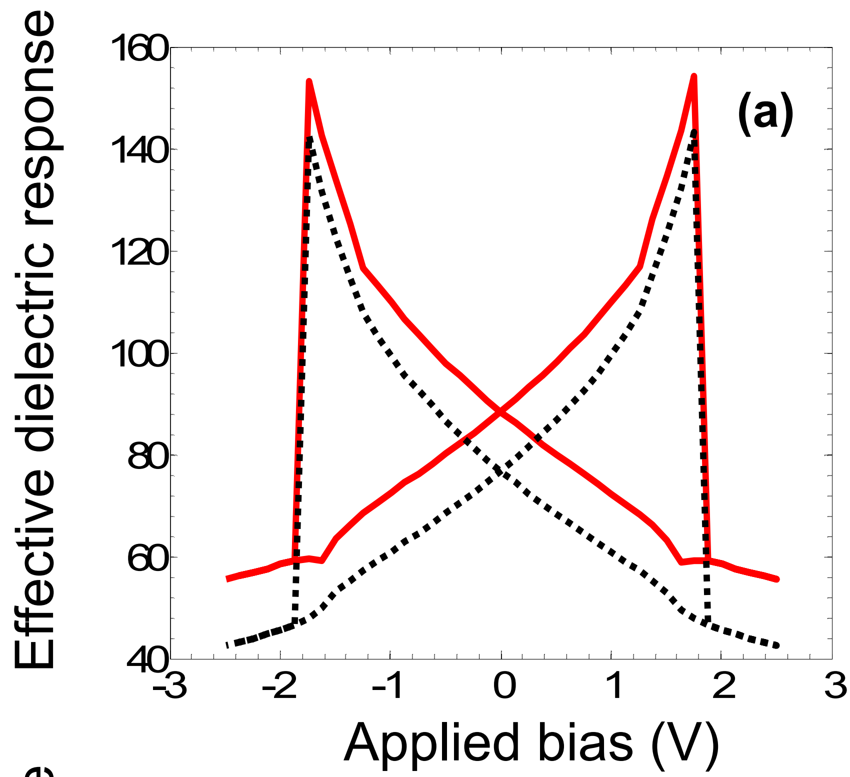

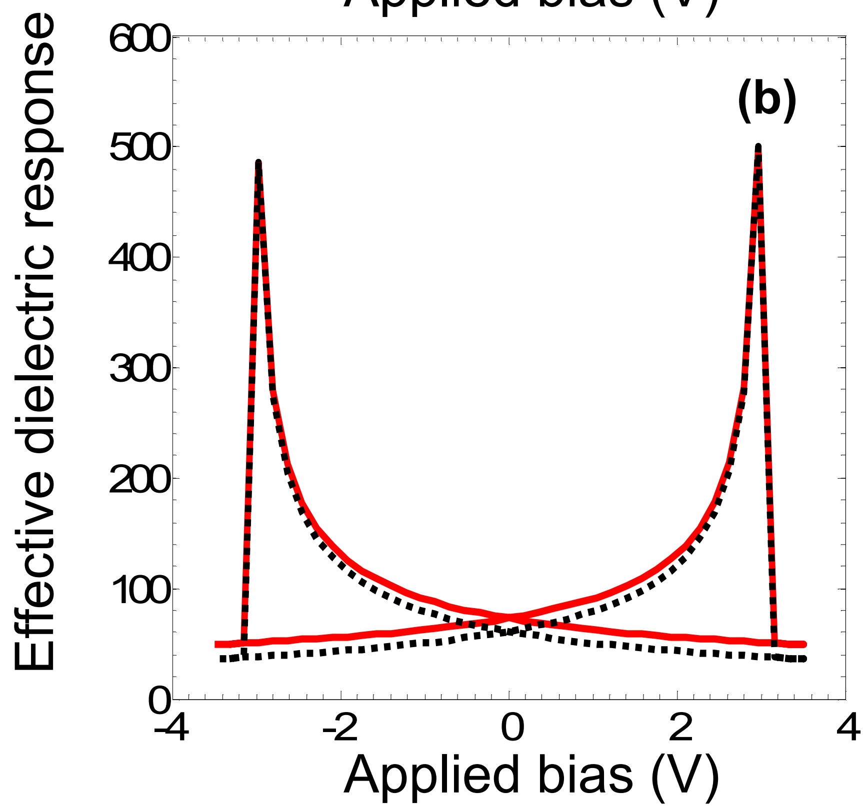

Figure 2. Misirlioglu and Yildiz

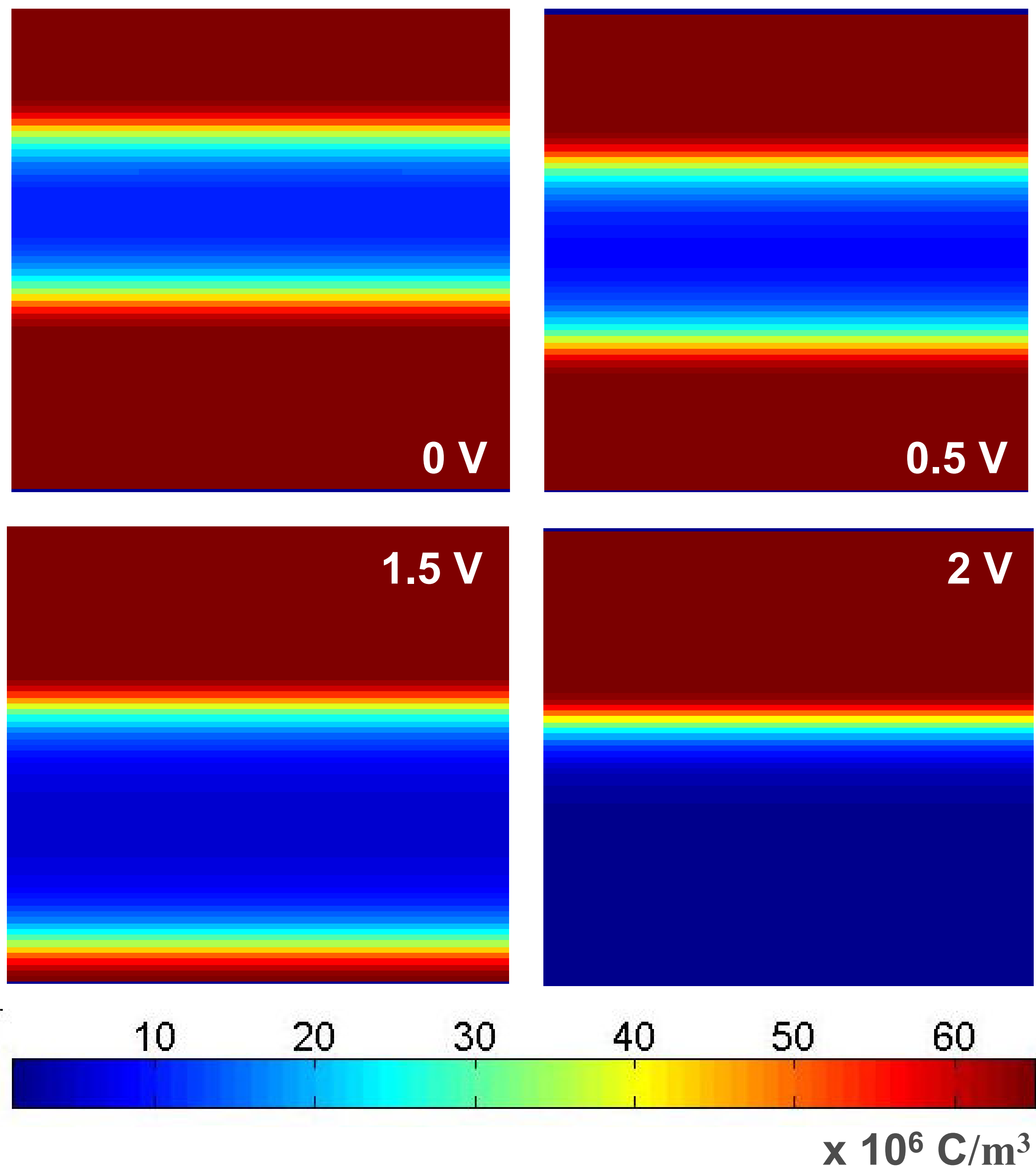

Figure 3. Misirlioglu and Yildiz

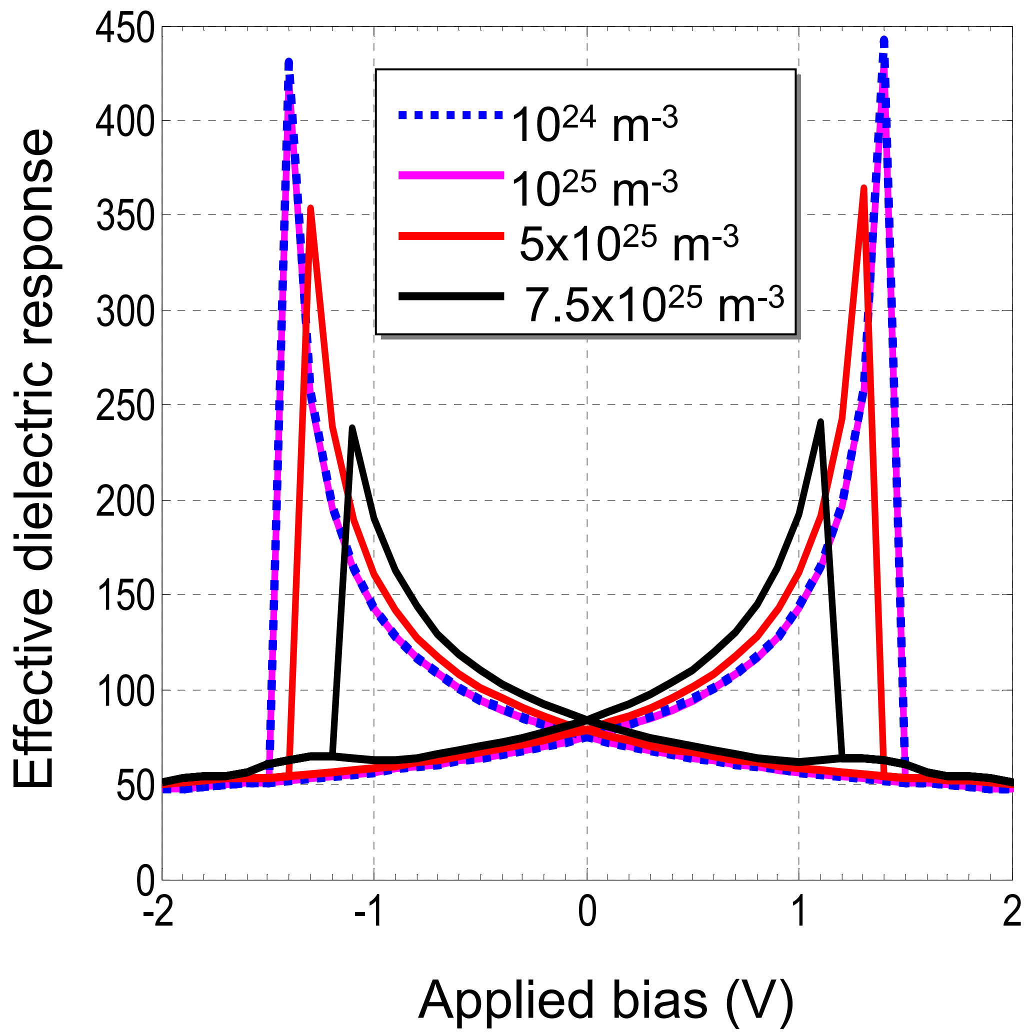

Figure 4. Misirlioglu and Yildiz

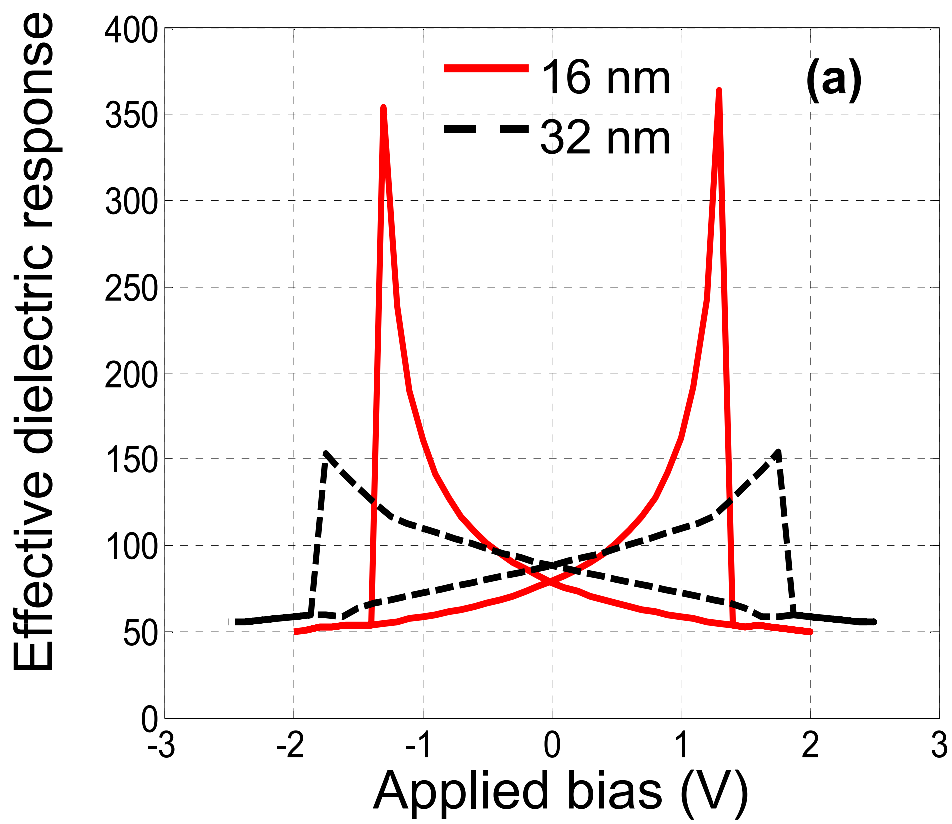

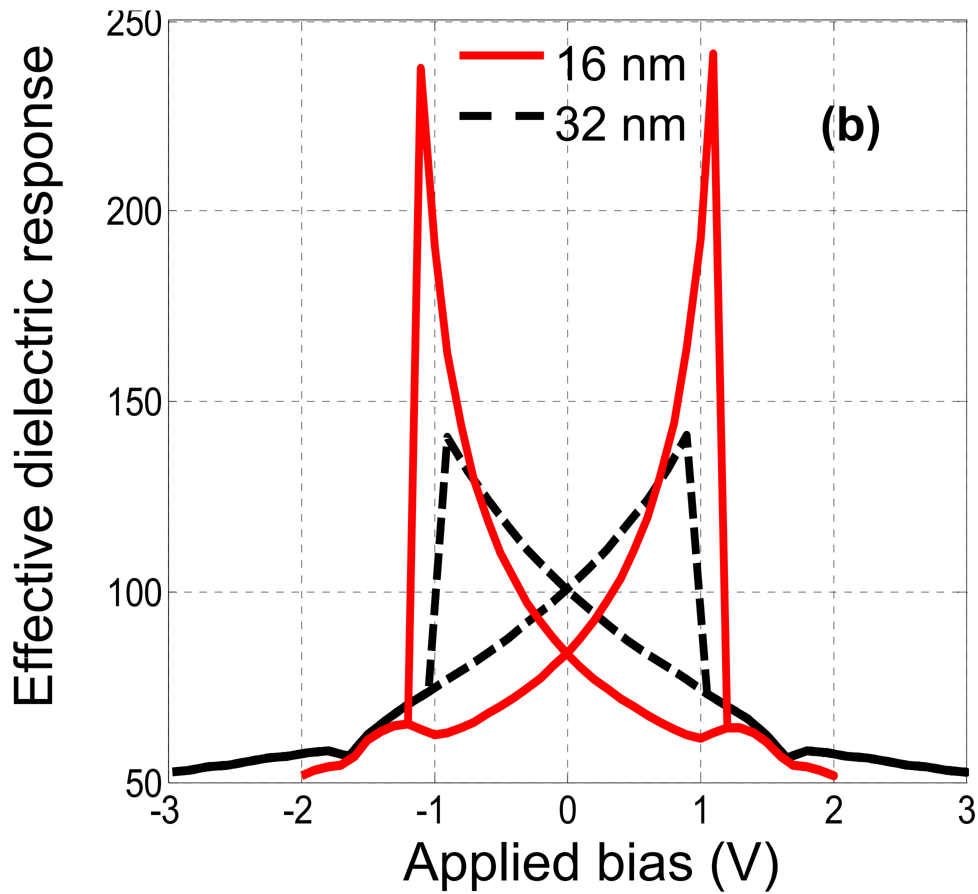

Figure 5. Misirlioglu and Yildiz

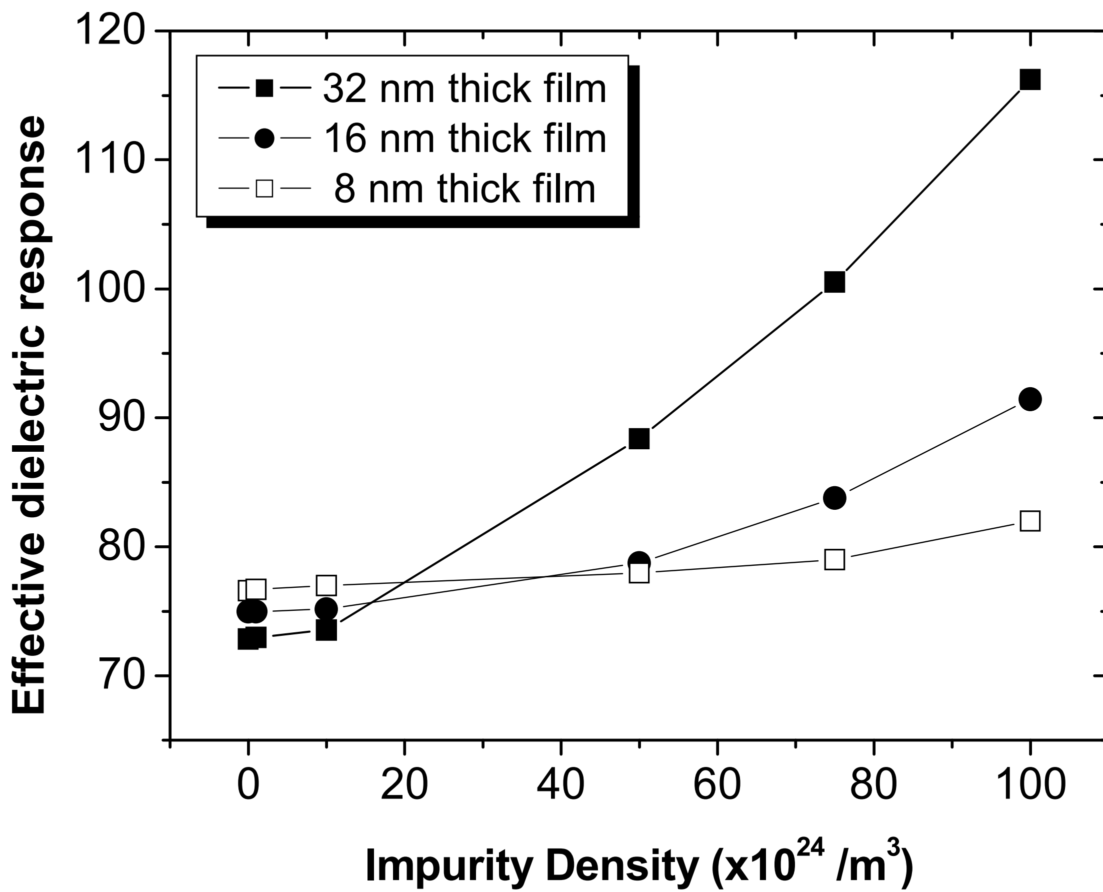

Figure 6. Misirlioglu and Yildiz

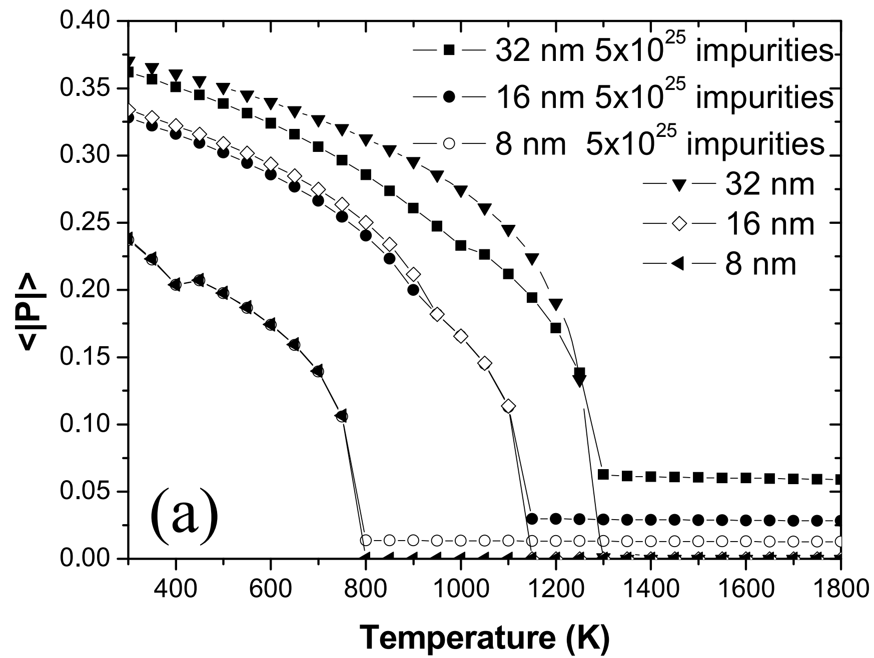

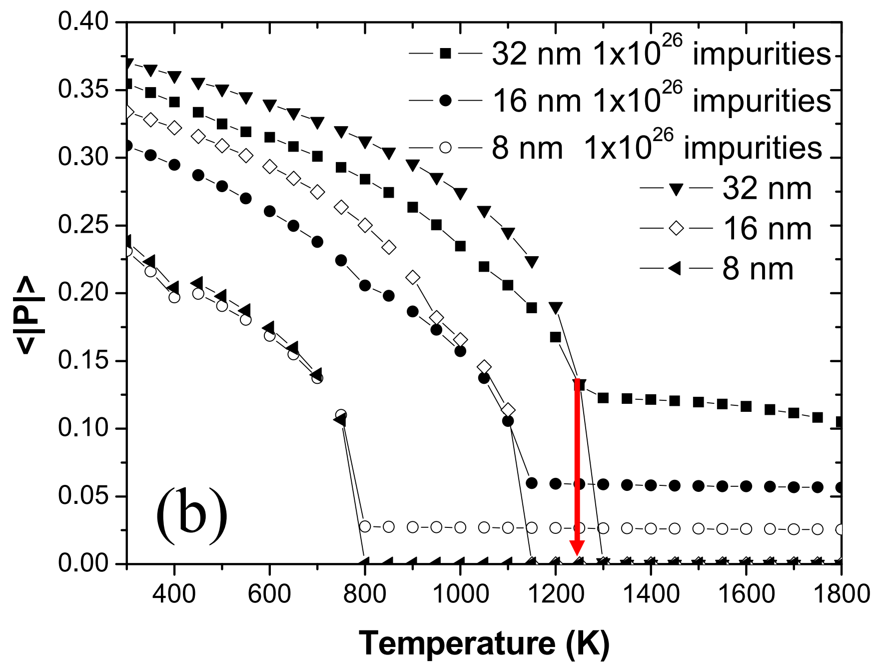

Figure 7. Misirlioglu and Yildiz

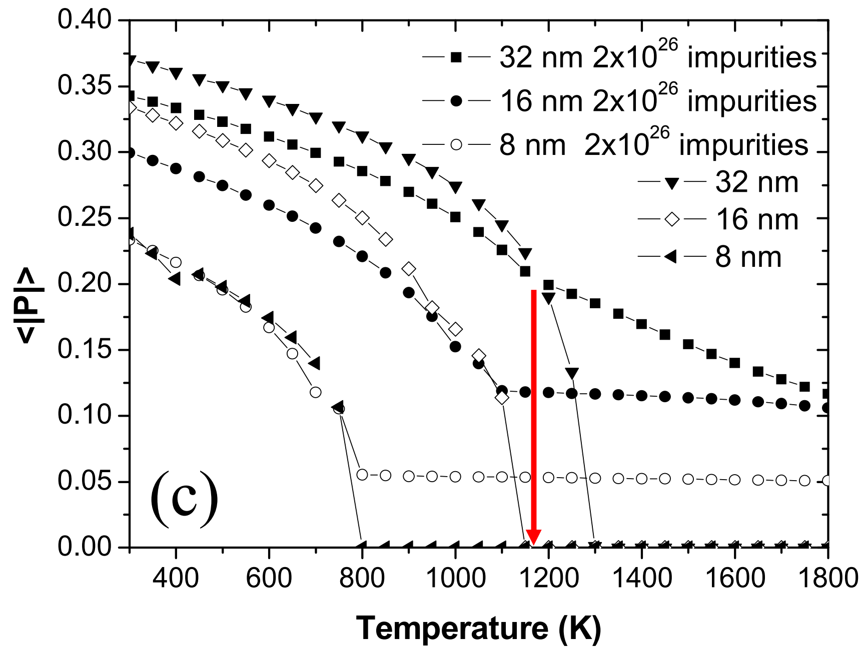

Figure 7. Misirlioglu and Yildiz